University of Sistan and Baluchestan

Chemical Process Design

Available online athttp://cpd.usb.ac.ir/

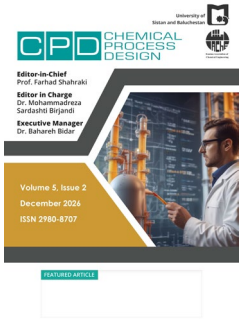

Domino Modeling of Process Events using the Graph Method and the Minimum Evolution Time Algorithm with Visibility Coefficient in Oil Product Storage Tanks in Sabzevar Region

Barat Mohammad Abbasiyan [1]✉, Abdolreza Moghadassi[2]

[1] Corresponding Author, Faculty of Engineering, Arak University. Email: b.abbasiyan.00@phd.araku.ac.ir
[2]Faculty of Engineering, Arak University. Email: a-moghadassi@araku.ac.ir

ARTICLE INFO

Article type:
Research Article

Article history:
Received: 2025-11-17
Received in revised form: 2026-03-30
Accepted: 2026-04-17
Available online: 2026-04-17

Keywords: *Domino; Simulation; PHAST; Storage tanks; Chemical processes*

ABSTRACT

One of the most critical threats to the safety and stability of process units is the occurrence of domino events triggered by fires or explosions. Accurate prediction of the temporal and spatial evolution of such events is therefore essential for safe facility layout design and emergency response planning. This study presents a dynamic numerical framework to forecast the spatio-temporal progression of fire-induced domino events in a cluster of petroleum product storage tanks located in the Sabzevar region. The model integrates the minimum evolution time algorithm with a graph-based structure to visualize tank ignition sequences. The heat radiation capability (HRC) serves as the primary escalation indicator, while a visibility coefficient is incorporated to refine the representation of thermal radiation transfer between tanks. Implemented in MATLAB, the model accepts inputs including tank geometry (type, dimensions, volume), product properties (burning rate), geographical coordinates, and HRC values derived from PHAST software, experimental data, or theoretical correlations. It supports both atmospheric and pressurized tanks (cylindrical or spherical) with no restrictions on tank count or layout complexity. Outputs include spatio-temporal event sequences, graphical overlays on offline satellite maps, and time-evolution tables. The results demonstrate high computational efficiency, enabling rapid data generation for emergency decision-making, quantitative domino risk assessment, and optimal tank placement.

Cite this article: Abbasiyan, B.M., Moghadassi, A., (2026), Domino Modeling of Process Events using the Graph Method and the Minimum Evolution Time Algorithm with Visibility Coefficient in Oil Product Storage Tanks in Sabzevar Region, *Chemical Process Design*, 5(2), 00-00. http//doi.org/10.22111/cpd.2026.53805.1080

DOI: http//doi.org/10.22111/cpd.2026.53805.1080

Publisher: University of Sistan and Baluchestan.

1. Introduction

The occurrence of industrial hazards is often inevitable and, in many cases, unpredictable [1]. High-risk industries including chemical, oil and gas, petrochemical, and related sectors—routinely involve the transfer, processing, separation, and storage of hazardous substances under diverse operating conditions [2]. Despite substantial progress in process safety science and engineering, major accidents continue to occur, frequently resulting in severe human, environmental, and economic consequences.

While significant advancements have been made in predicting and controlling isolated events, cascading domino effects—where an accident in one unit triggers successive failures in adjacent units—remain a critical safety concern [3]. Domino accidents are far from rare; a considerable proportion of major industrial incidents escalate due to these chain reactions. Explosions and fires are the most common initiating events, and their associated physical effects—thermal radiation, overpressure waves, and fragment projection—can propagate to nearby units, causing secondary and tertiary failures. The cumulative consequences of a domino chain often exceed those of the initiating event alone.

Comprehensive domino effect assessment requires detailed modeling of escalation mechanisms, quantitative probability estimation, and consequence analysis to identify vulnerable units and critical pathways [4]. A review of 225 historical domino accidents showed that explosions (57%) and fires (43%) were the primary initiating events. Storage areas account for approximately 35% of initiation sites, followed by process units (28%) and loading/unloading operations (19%). The most frequent escalation patterns include fire–explosion and fire–fire sequences [5]. Furthermore, Abdolhamidzadeh et al. reported that pool fires and flammable material releases constituted the dominant initiating scenarios in domino accidents [6].

Various analytical methodologies have been proposed to analyze domino effects, including probabilistic models, Bayesian networks, and Petri net approaches [7,8]. Among these, the Minimum Evolution Time (MET) algorithm introduced by Chen et al. [9] provides an efficient framework for modeling the spatial–temporal evolution of fire-induced domino effects using a graph-based representation.

However, the framework proposed by Chen et al. remained largely theoretical and lacked comprehensive numerical implementation in real industrial case studies. In addition, limited attention was given to the quantitative incorporation of inter-unit radiative obstruction effects. To address these limitations, the present study develops a fully operational MATLAB-based model that extends the MET framework by integrating empirical correlations, PHAST-derived radiation data, and a geometrically computed visibility coefficient to improve the accuracy of thermal radiation transfer between tanks.

The proposed model is validated using a petroleum storage case study in the Sabzevar region. It supports flexible simulation of both atmospheric and pressurized tanks (cylindrical or spherical) at arbitrary geographical locations using coordinate-based layouts. The framework is designed to provide rapid and reliable spatio-temporal predictions to support emergency decision-making, domino risk assessment, and optimized facility layout design.

2. Structure of the proposed model

2.1. Initial model data

To implement the proposed Minimum Evolution Time (MET) based framework, a set of geometric, thermophysical, and spatial parameters is required. These input parameters characterize the tank configuration and burning behavior and are defined as follows:

- Project identifier and total number of tanks under analysis
- Tank type, including geometric shape (cylindrical or spherical) and operating condition (atmospheric or pressurized)
- For cylindrical tanks: diameter and height (used to calculate volume and stored product mass)
- Product burning rate for each tank (kg/s)
- Geographic coordinates (latitude and longitude) of each tank

2.2. Location and graphical display of tank status

The geographical coordinates of tanks are converted into pixel positions using the latitude and longitude boundaries of an offline satellite map. This transformation enables graphical visualization of tank locations and dynamic status evolution.

At each time step, tank conditions are color-coded as follows:

- Blue: Normal (no thermal impact)
- Yellow: Receiving thermal radiation
- Red: Burning
- Black: Fire extinguished

This graphical interface allows the visualization of the spatio-temporal evolution of domino sequences.

2.3. Calculation of HRC (Heat Radiation Capability)

Within the MET framework, the Heat Radiation Capability (HRC) represents the radiative heat flux transmitted from a burning tank *i* to a target tank *j*. Two approaches are implemented for HRC estimation, depending on data availability.

2.3.1. Data from software simulation or experimental measurements

When detailed fire modeling data are available, thermal radiation intensity is extracted from PHAST simulations or validated experimental/field measurements.

Each tank is simulated individually, accounting for:

- Tank geometry and dimensions
- Product type
- Burning rate
- Wall height and configuration

Radiation intensity at various distances is extracted from PHAST output contours. The incident thermal radiation on adjacent tanks is then determined based on their relative spatial positions.

This approach provides high-fidelity radiation data and is used whenever reliable simulation or field measurements are available.

2.3.2. Theoretical method

In the absence of PHAST simulation data or experimental measurements, HRC is estimated using a simplified theoretical approach based on fundamental radiative heat transfer principles.

The flame is idealized as an isotropic point radiative source. Under this engineering approximation, the heat flux received by a target tank decreases proportionally to the inverse square of the center-to-center distance.

Accordingly, the radiative heat contribution from tank i to tank j is expressed as:

$$HRC_{i,j} = \frac{X_r \times q \times m_i}{4\pi R_{i,j}^2} \quad (1)$$

where:

$HRC_{i,j}$ = thermal radiation from tank i to tank j (kW/m²)

q = specific heat release rate of the product in tank i (kW/kg)

m_i = mass of product in tank i (kg)

$R_{i,j}$ = center-to-center distance between tanks i and j (m)

X_r = radiative fraction (dimensionless)

According to Mudan [11] and the radiative heat transfer literature, the radiative fraction for hydrocarbon pool fires typically ranges between 0.15 and 0.40. A representative mid-range value of 0.25 was adopted in this study. This formulation is employed only when detailed PHAST-derived radiation data are unavailable and serves as an engineering fallback estimation within the MET framework.

2.4. Calculation of the visibility coefficient between tanks

In dense tank farms, thermal radiation transfer between units may be partially obstructed by intermediate tanks. To account for geometric shielding effects, a visibility coefficient $VF_{i,j}$ is introduced. This parameter represents the fraction of radiant energy emitted from source tank i that reaches target tank j without obstruction.

2.4.1. Numerical evaluation of the visibility coefficient

The visibility coefficient is computed using a three-dimensional geometric ray-tracing approach. The effective radiating surface of the source tank and the corresponding receiving surface of the target tank are discretized into a 15 × 15 grid, resulting in 225 sampling points per surface. For each pair of sampling points, a hypothetical straight ray is traced. Rays that are not intercepted by intermediate tanks are classified as open paths, whereas rays blocked by other tanks are classified as closed paths. The visibility coefficient is defined as:

$$VF_{i,j} = \frac{N_{open}}{N_{total}} \quad (2)$$

where:

N_{open} = number of unobstructed ray paths

N_{total} = total number of sampled ray paths

This numerical approach enables a quantitative evaluation of geometric shielding effects.

2.4.2. Definition of effective radiating and receiving surfaces

The effective radiating surface depends on tank type:

For atmospheric cylindrical tanks, the effective emitting surface is modeled as a semi-cylinder (width = tank diameter D, height = tank height H). For pressurized spherical tanks, the effective emitting surface is modeled as a hemisphere (diameter = tank diameter). The receiving surface is defined as the half of the tank surface directly facing the source tank. A schematic representation of the discretization and ray-tracing procedure is shown in Fig. 1.

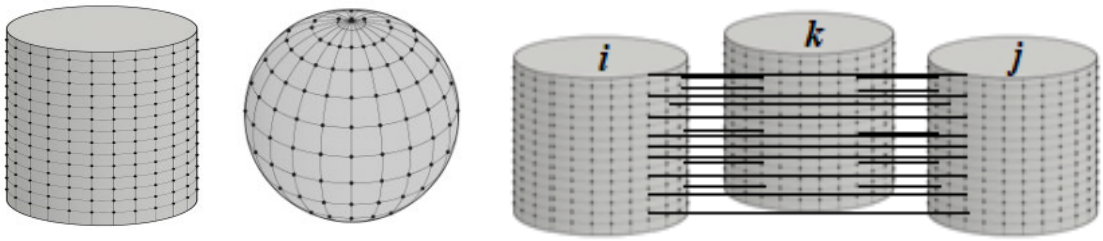

(a) (b)

Fig. 1. Schematic of the visibility coefficient calculation, (a) Sampling of spherical and cylindrical tanks with grid of 225 points (15×15) on the radiating and absorbing surfaces, (b) Ray tracing between source and target tanks to determine open paths

2.4.3. Integration of visibility into the HRC calculation

The obstruction-adjusted heat radiation capability is obtained by incorporating the visibility coefficient into the previously defined HRC expression:

$$HRC_{i,j}^{corr} = HRC_{i,j} \times VF_{i,j} \tag{3}$$

where, $HRC_{i,j}$ is the radiative heat flux calculated using Eq. (1) or simulation/ experimental data. $HRC_{i,j}^{corr}$ is the visibility-adjusted thermal radiation. Within the MET algorithm, $HRC_{i,j}^{corr}$ is used as the escalation parameter for ignition time calculation. Therefore, visibility directly influences the predicted domino sequence and ignition timing. This formulation is consistent with fundamental radiative heat transfer principles [12,13] and extends the qualitative visibility considerations of Landucci et al. [10] into a fully numerical framework.

2.5. Model algorithm

The computational procedure follows an iterative structure, as illustrated in Fig. 2. In this framework, the visibility-adjusted heat radiation capability (HRC), obtained from Eq. (3), serves as the input for calculating the total received heat (HR) of each target tank. Therefore, geometric obstruction effects are directly incorporated into the ignition sequence through the minimum evolution time (MET) algorithm.

For each non-ignited tank, the total received heat radiation is calculated as:

$$HR_j = \sum_{i=1}^{n} HRC_{i,j}, \left(j = 1,2,\ldots,n\right) \tag{4}$$

For the first iteration step ($m = 1$), the remaining failure time (RF) is determined as:

$$RF_j = \exp\left(-1.13\ln\left(HR_j\right) - 0.0000267V + 9.9\right), m = 1 \tag{5}$$

For subsequent iterations ($m>1$):

$$RF_j = \left(\frac{HR_j^m}{HR_j^{m-1}}\right)^{-0.95} \left(RF_j^{m-1} - t_{m-1}\right), m > 1 \tag{6}$$

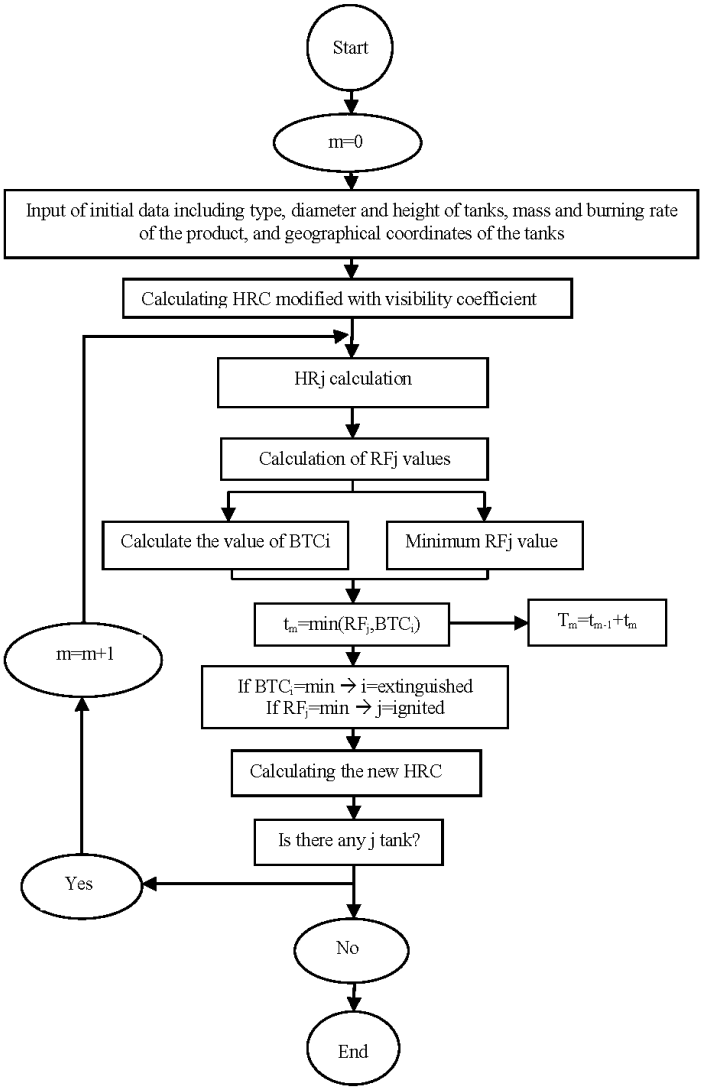

Fig. 2. Algorithm flowchart for the minimum evolution time considering the visibility coefficient

Due to the geometry-dependent characteristics of spherical tanks, the detailed formulation of their thermal radiation calculations is provided in Appendix A to avoid unnecessary expansion of the main text. Burning Time Capability (BTC) for tank i and the corresponding time step T_m are calculated as:

$$BTC_i = \frac{Product\ mass}{Burning\ rate} \tag{7}$$

$$T_m = \min\left(RF_j, BTC_i\right) \tag{8}$$

At each iteration step, the minimum value between the remaining failure time and the BTC determines the subsequent system evolution. The iterative process continues until no further domino escalation occurs. If BTC_i is the minimum value, tank i is considered extinguished. If RF_j is the minimum value, tank j is assumed to ignite. Fig. 2 presents the flowchart of the minimum evolution time algorithm incorporating the visibility coefficient.

2.6. Model computational and graphical outputs

At each iteration step of the simulation, tank statuses are updated dynamically and displayed on the satellite map according to the predefined color scheme. This graphical representation enables visualization of the spatio-temporal evolution of the domino event.

In addition to graphical outputs, the model generates tabulated results summarizing the minimum time values associated with state transitions, including heating, ignition, and extinguishment. The corresponding status of each tank at every time step is also recorded. The simulation environment allows the user to pause or terminate the analysis interactively, thereby providing flexibility for scenario evaluation and emergency response assessment.

3. Case study

3.1. Simulation implementation and analysis of the petroleum storage facility in the Sabzevar region

To evaluate the performance of the proposed model, it was applied to a real petroleum storage facility located in the Sabzevar region. The storage yard consists of 15 atmospheric cylindrical tanks containing diesel, gasoline, and kerosene. All tanks are vertical, fixed-roof, atmospheric storage vessels. The geometric and operational characteristics of the tanks—including dimensions, stored mass, product burning rate, and BTC—were implemented into the MATLAB model based on PHAST v6.5 output data. The detailed specifications are summarized in Table 1.

Table 1. Geometric and operational specifications of the 15 tanks used in the present model (based on PHAST output data)

Tanks No	Tanks type	Dimension (m)	Mass of product (kg)	Burn rate (kg/s)	BTC (min)
1	Cylindrical (atmospheric)	17.09×12.81	2060800	4.22	8139
2	Cylindrical (atmospheric)	17.09×12.81	2066400	4.22	8161
3	Cylindrical (atmospheric)	14.73×12.81	1823800	7.58	4010
4	Cylindrical (atmospheric)	14.73×12.81	1826000	7.58	4015
5	Cylindrical (atmospheric)	12.21×10.94	905280	1.98	7620
6	Cylindrical (atmospheric)	12.21×10.94	883200	1.98	7434
7	Cylindrical (atmospheric)	24.43×12.81	4931220	21.07	3900
8	Cylindrical (atmospheric)	24.43×12.81	4931220	21.06	3902
9	Cylindrical (atmospheric)	17.09×12.81	2420180	10.31	3912
10	Cylindrical (atmospheric)	17.09×12.81	2420180	10.31	3912
11	Cylindrical (atmospheric)	34.18×12.81	9086660	41.22	3674
12	Cylindrical (atmospheric)	34.18×12.81	8384200	18.00	7763
13	Cylindrical (atmospheric)	43.94×14.65	15866330	29.84	8861
14	Cylindrical (atmospheric)	34.18×12.81	9086660	42.75	3542
15	Cylindrical (atmospheric)	34.18×12.81	9075330	42.75	3538

3.2. Meteorological conditions used in PHAST simulations

Thermal radiation intensity values used as model inputs were extracted directly from PHAST consequence simulations. The simulations were conducted under defined atmospheric conditions corresponding to Pasquill Stability Class D (neutral atmospheric stability), which represents typical daytime neutral conditions in industrial environments. The adopted meteorological parameters were:

- Wind speed: 5m/s
- Atmospheric stability class: D (Pasquill classification)
- Ambient air temperature: 20°C
- Relative humidity: 70%
- Surface roughness: 0.1 m (industrial/open country terrain)

Stability Class D represents neutral atmospheric stratification and typically occurs under moderate wind conditions. In PHAST, this stability class affects plume behavior, atmospheric dispersion, and radiative attenuation. Therefore,

the radiation-versus-distance curves obtained from PHAST inherently incorporate the influence of wind speed, atmospheric turbulence, and environmental attenuation effects.

All radiation values applied in the present domino model correspond to these specified environmental conditions. Consequently, the spatio-temporal escalation results presented in this study are valid under the defined D/5 meteorological scenario.

3.3. Combustion Representation and Energy Release Assumption

The objective of the present framework is to predict domino ignition sequences and escalation timing rather than to simulate detailed transient combustion dynamics inside each storage tank.

For atmospheric cylindrical tanks subjected to pool fire conditions, combustion occurs at the liquid surface. In large-scale engineering fire modeling, the heat release rate (HRR) of pool fires is commonly correlated with the effective burning surface area and the product burning rate (kg/s per unit surface area).

Since the tank diameter remains constant during the fire and combustion is surface-controlled, the effective radiating surface area is assumed constant during the active burning phase of each tank.

Accordingly, in the present model:

- The instantaneous radiative output is determined based on the product burning rate and heat of combustion.
- The reduction of liquid level during burning is not explicitly modeled within the MET framework.
- The model does not dynamically adjust HRR based on instantaneous remaining mass.

It is important to clarify that the total energy released over the entire burning duration depends on the stored mass. However, for the purpose of radiation-driven domino propagation modeling, the instantaneous radiative heat flux is treated as surface-controlled and independent of progressive mass depletion during the burning period.

This assumption is consistent with standard engineering practice for large-scale pool fire modeling and ensures computational efficiency while preserving physical realism in ignition-time prediction.

3.4. Simulation and analysis using PHAST radiation data

PHAST v6.5 simulations were conducted for each product type (diesel, gasoline, kerosene) to obtain radiation intensity profiles as a function of distance from a burning tank under the defined meteorological conditions (D/5 scenario).

The resulting radiation-versus-distance curves are presented in Figs. 3(a)–(c). These curves served as direct inputs for calculating the Heat Radiation Capability (HRC) between tank pairs within the MET-based domino framework.

Following Abbasian et al. [14], Tank 13 was identified as the worst-case single-tank initiator due to its large storage capacity and product properties. A pool fire in Tank 13 was therefore selected as the initiating scenario.

The domino simulation outputs include:

- Time intervals for state transitions (Heating → Ignition; Ignition → Extinguishment) (Figs. 4(a)–(b)),
- Spatial tank state evolution at each domino step (Figs. 5(a)–(b)),
- Geographic visualization of domino progression overlaid on the Sabzevar satellite map (Appendix B),
- The complete matrix of calculated visibility coefficients (Appendix C).

All presented escalation timelines and ignition sequences correspond to the atmospheric and combustion assumptions defined above.

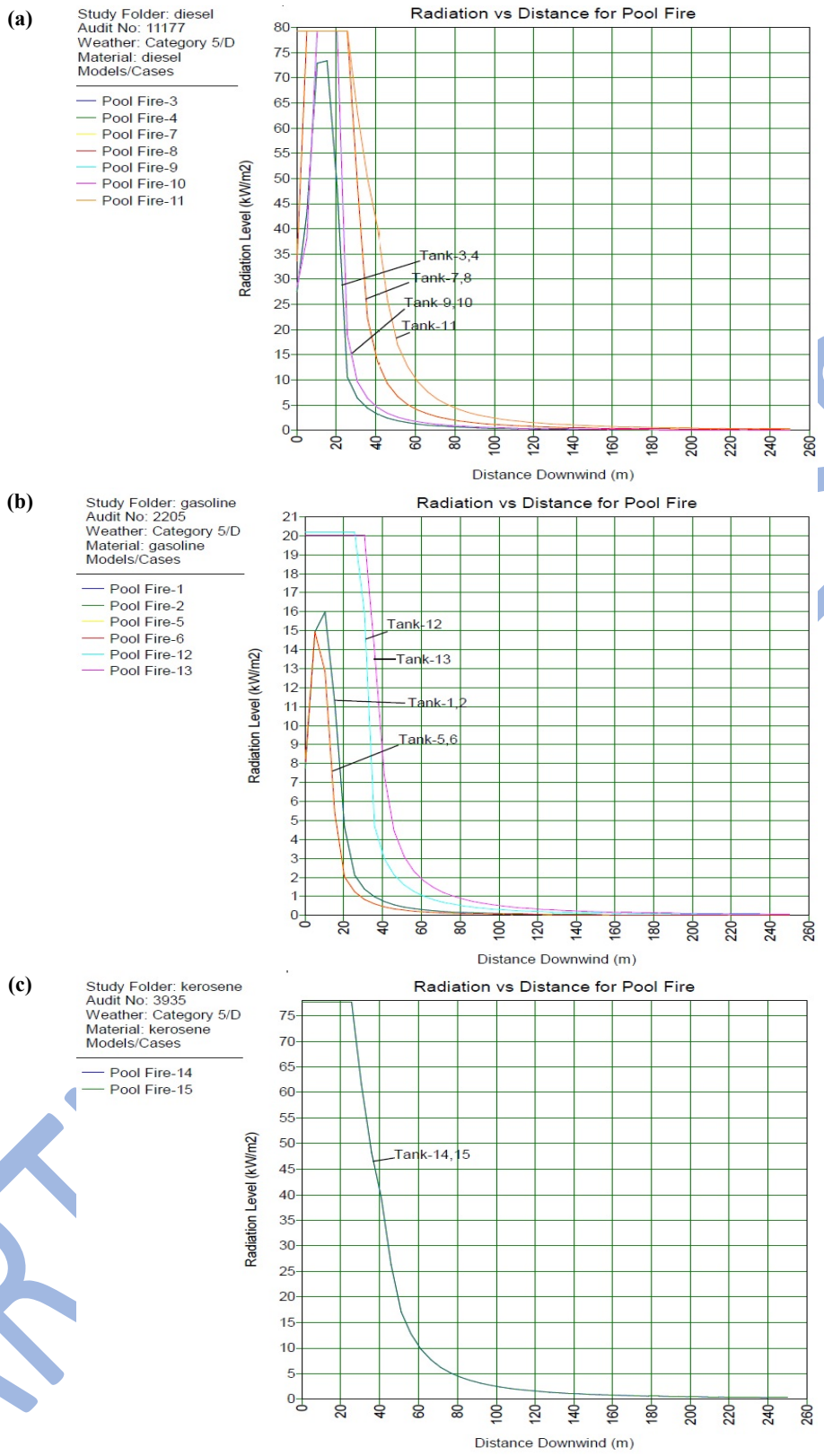

Fig. 3. Thermal radiation intensity as a function of distance from a burning tank for, (a) diesel, (b) gasoline, and (c) kerosene, based on PHAST v6.5 simulations

4. Sensitivity analysis

To evaluate the geometric sensitivity of the proposed framework, the center-to-center distance between tanks 13 and 12 was varied from 60m to 100m. Considering the combined tank radii (40m), the corresponding effective wall-to-wall separation ranged from 20m to 60m.

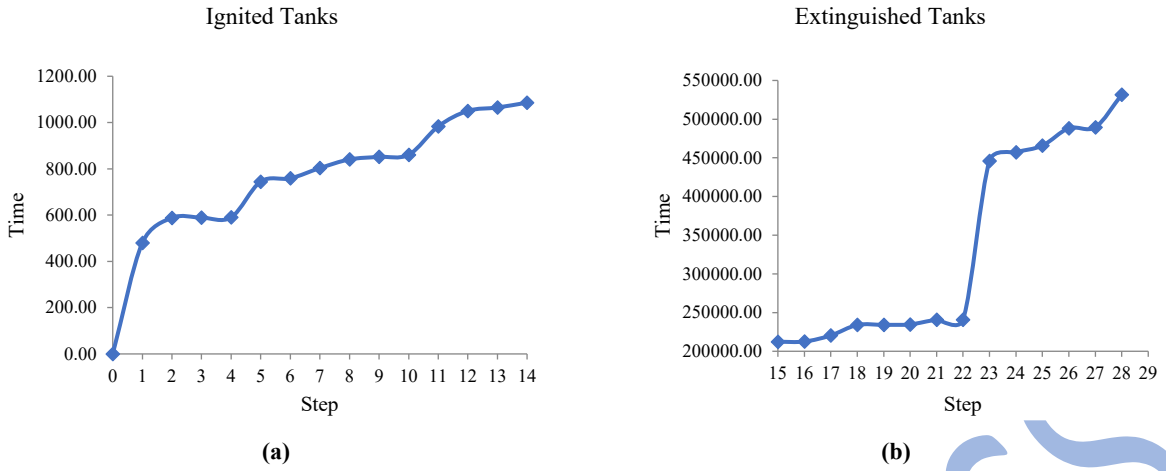

Fig. 4. The temporal evolution of each domino step: (a) transition from heating to ignition, (b) transition from ignition to extinguishment

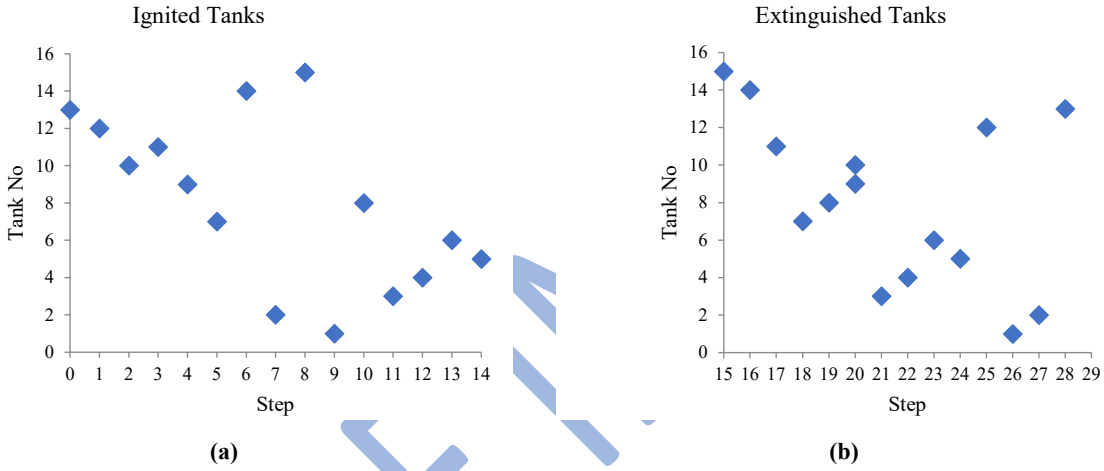

Fig. 5. The spatial distribution of tank states at each stage of the domino process: (a) during heating-to-ignition (b) during ignition-to-extinguishment

The results show that for wall-to-wall separations below 30m, the ignition time remains nearly constant at approximately 480s. This behavior indicates that the received thermal radiation significantly exceeds the ignition threshold under close-proximity conditions. As the separation distance increases beyond 30m, ignition time rises markedly. Increasing the wall-to-wall separation from 30m to 60m results in an increase in ignition time from 480s to 6659s, corresponding to a 1287% increase. This pronounced non-linear behavior confirms the strong dependence of ignition time on geometric separation and is physically consistent with the inverse-square radiation law governing point-source thermal emission. Fig. 6 illustrates the geometric sensitivity analysis results.

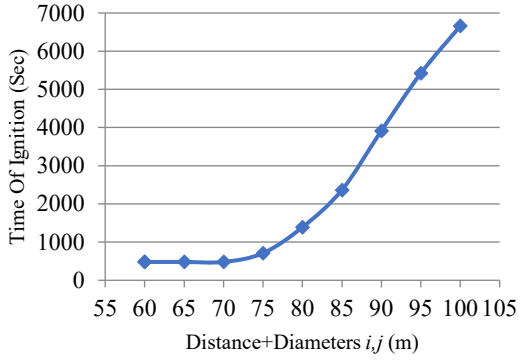

Fig. 6. Geometric sensitivity analysis

5. Model Validation

To assess the predictive accuracy of the proposed methodology, the simulation results were compared with ignition times reported in the reference study by Chen et al. [9]. The selected reference was chosen due to the comparable tank configuration, stored substance characteristics, and fire escalation scenario. In the present model, the ignition time of each tank was defined as the first time step at which its status changed from heating to ignited. These predicted values were directly compared with the ignition times reported in the reference model.

To quantify the deviation, the percentage difference was calculated for each comparable tank using:

$$Deviation(\%) = \frac{t_{present,i} - t_{ref,i}}{t_{ref,i}} \times 100 \quad (9)$$

where $t_{present}$ represents the ignition time predicted by the present model and t_{ref} denotes the ignition time reported in the reference study. (Tank T5 ignites at t = 0). The comparison indicates perfect agreement (0% deviation) for Tanks T3 and T4. For Tank T2, a time difference of 58.71s was observed, corresponding to a deviation of 4.21%, which remains within an acceptable range for domino-effect prediction models.

For Tank T1, the reference study reported an ignition time of 1335.83s, whereas no ignition occurred in the present simulation. This discrepancy is attributed to the explicit incorporation of the visibility coefficient and radiative obstruction effects in the proposed model, which reduced the incident heat flux received by this tank. In contrast, the reference model assumed full radiative exposure without accounting for geometric obstruction.

The mean deviation among the directly comparable tanks (T2–T4) was 1.40%, demonstrating the high predictive capability of the proposed methodology in terms of both ignition sequence and ignition timing.

Overall, the results confirm that the proposed framework not only reproduces the general domino propagation pattern reported in the literature but also provides quantitatively consistent ignition predictions with limited numerical deviation. Table 2 presents a step-by-step comparison between the Chen et al. [9] model and the present model.

Table 2. Comparison of results from Chen et al. [9] model and the present model

Chen et al. [9] model								
Step	**Time**	**Ignited_1**	**Ignited_2**	**Ignited_3**	**Ignited_4**	**Heated_1**	**Heated_2**	**Heated_3**
0	0	5						
1	881.79	5	3			1	2	4
2	1101.56	3				1	2	4
3	1149.09	3	4			1	2	
4	1335.83	3	4	1		2		
5	1396.13	3	4	1	2			
6	8372.29	3	4	1				
7	10281.27	3	1					
8	22031.28	1						
9	24419.17							
Present model								
Step	**Time**	**Ignited_1**	**Ignited_2**	**Ignited_3**	**Ignited_4**	**Heated_1**	**Heated_2**	**Heated_3**
0	0	5						
1	881.79	5	3			1	2	4
2	1101.56	5				1	2	4
3	1149.09	3	4			1	2	
4	1454.84	3	4	2		1		
5	8372.29	3	4			1		
6	10281.27	3				1		
7	22031.28	0	0	0	0	1		

6. Discussion

The integration of the visibility coefficient into the minimum evolution time algorithm has markedly improved the physical realism of spatio-temporal domino event predictions. Unlike the model by Chen et al. [9], which assumed unobstructed radiation transfer between all tank pairs, the present framework numerically quantifies the fraction of radiant energy reaching each target tank by accounting for geometric obstructions.This refinement yields more accurate heat flux estimates, resulting in closer alignment between simulated and physically plausible escalation sequences. A key example is the non-ignition of tank 1 in the proposed model. Due to partial shielding by intermediate tanks, the visibility coefficient reduced the effective thermal radiation below the failure threshold. This outcome not only demonstrates the model's sensitivity to layout geometry but also highlights its practical implications for facility design and emergency response planning.The model's computational efficiency enables rapid scenario analysis, making it a valuable tool for quantitative domino risk assessment across oil, gas, petrochemical, and chemical industries. It supports layout optimization, fire-spread forecasting, and real-time decision-making during emergency scenarios.

7. Conclusion

This study developed and validated a dynamic MATLAB-based model for simulating fire-induced domino events in petroleum storage facilities. By coupling the minimum evolution time algorithm with a graph-theoretic structure and a numerically computed visibility coefficient, the model accurately predicts ignition sequences and escalation timelines under complex geometric constraints. When applied to a real-world cluster of 15 atmospheric cylindrical tanks in the Sabzevar region, the model demonstrated high fidelity with PHAST-derived radiation data and superior physical consistency compared to prior approaches. The visibility coefficient proved critical in preventing overestimation of heat transfer in obstructed configurations.The framework is fully generalizable: it accommodates any number and type of tanks (cylindrical or spherical, atmospheric or pressurized), arbitrary stored products, and user-defined geographical coordinates. Its outputs—spatio-temporal event maps, state-transition tables, and escalation timelines—support proactive risk mitigation and emergency management.Future work should incorporate wind-driven convection, explosion overpressure, toxic dispersion, and multi-phase heat transfer to enhance predictive accuracy in diverse industrial settings.

Nomenclature

Symbols

q	Specific heat release rate (kW/kg)
X_r	Radiative fraction (dimensionless)
R	Center-to-center distance (m)
m	Mass of product (kg)
V	Tank Volume (m^3)
T,t	Time (sec)
D	Pasquill classification (dimensionless)

Abbreviation

HRC	Heat Radiation Capability
MET	Minimum Evolution Time
VF	Visibility Coefficient
HR	Heat Radiation
RF	Remaining Failure Time
BTC	Burning Time Capability
HRR	Heat Release Rate

References

[1] Lees, F. P., 2005. Lees' loss prevention in the process industries, Hazard identification, assessment and control, 3rd Edition, Elsevier.

[2] Marin, P., Tambourgi, E., 2009. Risk analysis and environmental impact analysis in a chemical processing facility, Proceedings of the 10th International Symposium on Process Systems Engineering (PSE).

[3] Abdolhamidzadeh, B., Abbasi, T., Rashtchian, D., Abbasi, S. A., 2010. A new method for assessing domino effect in chemical process industry, Journal of Hazardous Materials, 182, 416–426. https://doi.org/10.1016/j.jhazmat.2010.06.049

[4] George, P. G., Renjith, V. R., 2019. Quantitative assessment and consequence modeling of deliberately induced domino effects in process facilities. Proceedings of the Mary Kay O'Connor Process Safety Center, 22nd Annual International Symposium, October 22–24.
[5] Kadri, F., Chatelet, E., 2013. Domino effect analysis and assessment of industrial sites: A review of methodologies and software tools, International Journal of Computers and Distributed Systems, 2(3), 1–10.
[6] Abdolhamidzadeh, B., Abbasi, T., Rashtchian, D., Abbasi, S. A., 2011. Domino effect in process-industry accidents: An inventory of past events and identification of some patterns, Journal of Loss Prevention in the Process Industries, 24, 575–593. https://doi.org/10.1016/j.jlp.2010.06.013
[7] Kamil, M. Z., Taleb-Berrouane, M., Khan, F., Ahmed, S., 2019. Dynamic domino effect risk assessment using Petri-nets, Process Safety and Environmental Protection, 132, 113–128. https://doi.org/10.1016/j.psep.2019.02.019
[8] Khakzad, N., Amyotte, P., Cozzani, V., Reniers, G., Pasman, H., 2018. How to address model uncertainty in the escalation of domino effects?, Journal of Loss Prevention in the Process Industries, 54, 459–473. https://dx.doi.org/10.1016/j.jlp.2018.03.001
[9] Chen, C., Reniers, G., Zhang, L., 2020. An innovative methodology for quickly modeling the spatial–temporal evolution of domino accidents triggered by fire, Process Safety and Environmental Protection, 143, 170–183. https://doi.org/10.1016/j.jlp.2018.04.012
[10] Landucci, G., Gubinelli, G., Antonioni, G., Cozzani, V., 2009. The assessment of the damage probability of storage tanks in domino events triggered by fire, Accident Analysis and Prevention, 41(6), 1206–1215. https://doi.org/10.1016/j.aap.2008.05.006
[11] Mudan, K.S., 1984. Thermal radiation hazards from hydrocarbon pool fires, Progress in Energy and Combustion Science 10(1), 59–80. https://doi.org/10.1016/0360-1285(84)90019-9
[12] Modest, M. F., 2013. Radiative heat transfer, 3rd edition, Academic Press. https://doi.org/10.1016/C2010-0-66234-7
[13] Siegel, R., Howell, J. R., Mengüç, M. P., 2015. Thermal radiation heat transfer, 6th edition, CRC Press. https://doi.org/10.1201/b18835
[14] Abbasian, B. M., Khalilipoor, M. M., Shahraki, F., 2014. Modeling of release consequences of petroleum products from storage tanks in the National Iranian Oil Products Distribution Company, Sabzevar region, Proceedings of the National Conference on Environmental Sciences and Engineering, Ahvaz, Iran. [In Persian]. https://civilica.com/doc/366140

Appendix A. The detailed formulation of thermal radiation calculations for spherical tanks

For spherical tanks Eq. (5) and Eq. (6) will change as below:

Eq. (5) for spherical tank:

$$RF_j = \exp\left(-1.05\ln\left(HR_j\right) - 0.000032V + 8.5\right), m = 1 \tag{A.1}$$

Eq. (6) for spherical tank:

$$RF_j = \left(\frac{HR_j^m}{HR_j^{m-1}}\right)^{-1.13}\left(RF_j^{m-1} - t_{m-1}\right), m > 1 \tag{A.2}$$

Appendix B. Geographical map of the Sabzevar region

Geographical map of the Sabzevar region showing simulation stages from the initial scenario (Tank 13 ignition) to domino process completion, with color-coded tank status (blue: normal, yellow: heated, red: ignited, black: extinguished).

Fig B.1. Geographical map of the Sabzevar region showing simulation stages from the initial scenario (Tank 13 ignition) to domino process completion, with color-coded tank status (blue: normal, yellow: heated, red: ignited, black: extinguished)

Appendix C. Visibility coefficients

The complete set of calculated visibility coefficients as a numerical matrix using 225 points on tank surfaces (15×15points) with Matlab Program.

Table C.1. The complete set of calculated visibility coefficients

i,j	T-1	T-2	T-3	T-4	T-5	T-6	T-7	T-8	T-9	T-10	T-10	T-12	T-13	T-14	T-15
T-1	0.00	1.00	1.00	1.00	0.00	0.60	1.00	1.00	0.13	0.07	1.00	0.30	0.01	0.17	0.28
T-2	1.00	0.00	1.00	1.00	1.00	0.00	1.00	0.97	1.00	1.00	1.00	0.95	0.47	1.00	0.74
T-3	1.00	1.00	0.00	1.00	1.00	1.00	0.00	0.13	1.00	1.00	1.00	0.00	0.14	1.00	0.64
T-4	1.00	1.00	1.00	0.00	1.00	1.00	0.00	0.34	0.11	0.78	0.00	0.04	0.17	0.37	0.17
T-5	0.00	1.00	1.00	1.00	0.00	1.00	0.00	0.12	0.80	0.00	0.00	0.00	0.09	0.55	0.03
T-6	0.60	0.00	1.00	1.00	1.00	0.00	0.00	0.00	1.00	1.00	1.00	0.00	0.39	1.00	0.31
T-7	1.00	1.00	0.00	0.00	0.00	0.00	0.00	1.00	1.00	1.00	1.00	0.00	0.45	0.72	0.22
T-8	1.00	0.97	0.13	0.34	0.12	0.00	1.00	0.00	0.80	0.45	0.04	0.00	0.19	0.21	0.08
T-9	0.13	1.00	1.00	0.11	0.80	1.00	1.00	0.80	0.00	1.00	0.00	1.00	1.00	1.00	1.00
T-10	0.07	1.00	1.00	0.78	0.00	1.00	1.00	0.45	1.00	0.00	1.00	1.00	1.00	0.58	0.53
T-11	1.00	1.00	1.00	0.00	0.00	1.00	1.00	0.04	0.00	1.00	0.00	1.00	1.00	0.58	0.00
T-12	0.30	0.95	0.00	0.04	0.00	0.00	0.00	0.00	1.00	1.00	1.00	0.00	1.00	0.00	0.40
T-13	0.01	0.47	0.14	0.17	0.09	0.39	0.45	0.19	1.00	1.00	1.00	1.00	0.00	1.00	1.00
T-14	0.17	1.00	1.00	0.37	0.55	1.00	0.72	0.21	1.00	0.58	0.58	0.00	1.00	0.00	1.00
T-15	0.28	0.74	0.64	0.17	0.03	0.31	0.22	0.08	1.00	0.53	0.00	0.40	1.00	1.00	0.00